Geol. Mag. **141** (*4*), *2004, pp. 401–416. © 2004 Cambridge University Press*
DOI: 10.1017/S0016756804009409 *Printed in the United Kingdom*

Organic-carbon deposition in the Cretaceous of the Ionian Basin, NW Greece: the Paquier Event (OAE 1b) revisited

HARILAOS TSIKOS*†, VASILIOS KARAKITSIOS‡, YVONNE VAN BREUGEL§, BEN WALSWORTH-BELL¶, LUCA BOMBARDIERE‖, MARIA ROSE PETRIZZO¶, JAAP S. SINNINGHE DAMSTÉ§, STEFAN SCHOUTEN§, ELISABETTA ERBA¶, ISABELLA PREMOLI SILVA¶, PAUL FARRIMOND‖, RICHARD V. TYSON‖ & HUGH C. JENKYNS*

*Department of Earth Sciences, University of Oxford, Parks Road, Oxford OX1 3PR, UK
‡Department of Geology, University of Athens, Panepistimiopolis 15784, Athens, Greece
§Department of Marine Biogeochemistry & Toxicology, Royal Netherlands Institute for Sea Research (NIOZ), 1790 AB Den Burg, The Netherlands
¶Department of Earth Sciences 'Ardito Desio', University of Milan, Via L. Mangiagalli 34, 20133 Milano, Italy
‖NRG, School of Civil Engineering & Geosciences, Drummond Building, University of Newcastle, Newcastle upon Tyne NE1 7RU, UK

(*Received* 11 August 2003; *accepted* 20 January 2004)

Abstract – We present new stable (C, O) isotopic, biostratigraphic and organic geochemical data for the Vigla Shale Member of the Ionian Zone in NW Greece, in order to characterize organic carbon-rich strata that potentially record the impact of Cretaceous Oceanic Anoxic Events (OAEs). In a section exposed near Gotzikas (NW Epirus), we sampled a number of decimetre-thick, organic carbon-rich units enclosed within marly, locally silicified, Vigla Limestone (Berriasian–Turonian). All these units are characterized by largely comparable bulk geochemical characteristics, indicating a common marine origin and low thermal maturity. However, the stratigraphically highest of these black shales is further distinguished by its much higher total organic-carbon (TOC) content (28.9 wt%) and Hydrogen Index (HI) (529), and much enriched $\delta^{13}C_{org}$ value (−22.1‰). Planktonic foraminiferal and calcareous nannofossil biostratigraphy indicate a lower to middle Albian age for the strata immediately above, and a lower Aptian age for the strata below, the uppermost black shale. In terms of molecular organic geochemistry, the latter black shale is also relatively enriched in specific isoprenoidal compounds (especially monocyclic isoprenoids), whose isotopic values are as high as −15‰, indicating a substantial archaeal contribution to the organic matter. The striking similarities between the molecular signatures of the uppermost Vigla black shale and coeval organic-rich strata from SE France and the North Atlantic (ODP Site 1049C) indicate that this level constitutes a record of the Paquier Event (OAE 1b).

Keywords: Cretaceous, Albian, stratigraphy, isotopes, carbon.

1. Introduction

The western Hellenides constitute part of the southern passive continental margin of the early Mesozoic to mid-Cenozoic Tethyan Ocean. Within this domain, a number of argillaceous–siliceous and organic carbon-rich units are associated with pelagic carbonate series (Bernoulli & Jenkyns, 1974; Chiotis, 1983; Jenkyns, 1988; Baudin & Lachkar, 1990; Karakitsios, 1995; Karakitsios & Rigakis, 1996; Rigakis & Karakitsios, 1998; Neumann & Zacher, 2004). Some of these organic-rich sediments may be causally linked to widespread Oceanic Anoxic Events (OAEs), as originally defined by Schlanger & Jenkyns (1976) for the Mesozoic. OAEs define periods during which much of the world's oceans became severely depleted in oxygen and widespread deposition of organic carbon-rich shales took place (Jenkyns, 1980). The driving mechanism of OAEs is still the subject of much controversy and suggested possibilities include, amongst others, increased primary production, expansion of the oxygen-minimum zone, water-column stratification, large-scale volcanism, and/or episodic release of gas hydrates, either singly or in combination (Jenkyns, 1999, 2003; Larson & Erba, 1999; Jones & Jenkyns, 2001). In many cases there is organic geochemical evidence for sulphate reduction in the higher levels of the water column during the most intense phases of OAEs (Sinninghe Damsté & Köster, 1998; Kuypers *et al*. 2002*b*; Pancost *et al*. 2004).

The organic-rich intervals cropping out in the Ionian Zone in northwestern Greece are contained within the Albian–Cenomanian Vigla Shale Member or

† Author for correspondence: h.tsikos@abdn.ac.uk; present address: Department of Geology & Petroleum Geology, University of Aberdeen, Aberdeen AB24 3UE, UK.

'Upper Siliceous Zone' of the Vigla Limestone Formation (IGRS-IFP, 1966; Karakitsios, 1995; Rigakis & Karakitsios, 1998). Although certain lithological and organic geochemical aspects of such horizons in the Vigla Shale Member have already been reported (e.g. Rigakis & Karakitsios, 1998), no combined stratigraphic and geochemical studies in the context of Oceanic Anoxic Events have hitherto been undertaken.

In this paper, we present new chemostratigraphic, biostratigraphic and organic geochemical data from a section of the Vigla Shale Member in the Gotzikas area in NW Epirus, Greece. These results provide insights into the palaeoenvironmental setting of the Vigla sediments, and facilitate comparisons and correlation with analogous organic-rich sequences deposited in the Tethys and Atlantic oceans.

2. Regional geological framework

The Ionian Zone of northwestern Greece (Epirus region) constitutes part of the most external zones of the Hellenides (Paxos Zone, Ionian Zone, Gavrovo Zone; Fig. 1a). These zones correspond to the Hellenic domain of the southern passive continental margin associated with early Mesozoic opening and late Mesozoic–early Cenozoic closure of the Neotethyan Ocean (Laubscher & Bernoulli, 1977; Karakitsios, 1992, 1995). The rocks of the Ionian Zone range from Triassic evaporites and associated breccias through a varied series of Jurassic through upper Eocene carbonates and lesser cherts and shales, followed by Oligocene flysch (Fig. 2).

During the early Lias, the present part of northwestern Greece was covered by an extensive carbonate platform (Bernoulli & Renz, 1970; Karakitsios, 1992, 1995). The contemporaneous, shallow-water Pantokrator limestones (Aubouin, 1959; IGRS-IFP, 1966; Karakitsios, 1990, 1992) represent the pre-rift sequence of the Ionian Basin. These limestones overlie early to middle Triassic evaporites, probably related to the initial rifting of the Neotethyan Ocean, through Foustapidima Limestones of Ladinian–Rhaetian age (Renz, 1955; Pomoni-Papaioannou & Tsaila-Monopolis, 1983; Dragastan, Papanikos & Papanikos, 1985; Karakitsios & Tsaila-Monopolis, 1990).

During the Pliensbachian, extensional stresses associated with the opening of the Neotethyan Ocean brought about the formation of the Ionian Basin (Karakitsios, 1992, 1995). Although production of platform carbonates persisted through the entire Jurassic period in the adjacent Paxos (pre-Apulian) and Gavrovo-Tripolitza zones, the Ionian Basin became an area of more persistent syn-sedimentary faulting and subsidence. A syn-rift sequence began with deposition of the Siniais Limestones and their lateral equivalent, the Louros Limestones (Karakitsios & Tsaila-Monopolis, 1988; Dommergues *et al*. 2002). These formations record regional subsidence, which was followed by internal syn-rift differentiation of the Ionian Basin into smaller palaeogeographic units. The latter are recorded by the prismatic syn-sedimentary wedges of the syn-rift formations, and include the Louros Limestones, the Ammonitico Rosso or Lower Posidonia Beds, the 'Limestones with Filaments' and the Upper Posidonia Beds (Karakitsios, Danelian & De Wever, 1988; Karakitsios, 1995; see Fig. 2).

The early Berriasian was defined by a break-up marked by an unconformity at the base of the pelagic Vigla Limestone Formation; in this post-rift period sedimentation was relatively uniform across the whole Ionian Basin (Karakitsios, 1990; Karakitsios & Koletti, 1992). The post-rift sequence (Vigla Limestones and overlying Alpine formations) largely obscures the syn-rift structures and, in some cases, directly overlies the Pantokrator limestone pre-rift sequence (Karakitsios, 1992, 1995). This palaeogeographic configuration continued with minor off- and onlap movements along the basin margin until the late Eocene, when orogenic movements and flysch sedimentation began. The permanence of differential subsidence during the deposition of the post-rift sequence, shown by the strong variation in thickness of these formations, is probably due to the halokinetic movements of the Ionian Zone evaporitic base (IGRS-IFP, 1966; Karakitsios, 1990, 1992). The particular geometry of the restricted sub-basins that were formed during the syn-rift and post-rift period of the Ionian Zone may have favoured increased organic matter burial during the early Toarcian, late Callovian–Tithonian (Posidonia Beds) and Aptian–Cenomanian (Vigla Shale Member) (Karakitsios, 1995; Rigakis & Karakitsios, 1998). Some of these intervals, in fact, appear to record global rather than local events, as is the case with the early Toarcian (Jenkyns, 1988; Jenkyns *et al*. 2002) and early Aptian (Danelian *et al*. 2004).

3. The Gotzikas Section

The Vigla Limestone Formation (Berriasian–Turonian) consists of thinly bedded, white to grey micritic packstone, rhythmically alternating with chert layers and containing rare intercalations of shale. The Vigla Shale Member constitutes part of the Vigla Limestone Formation (Fig. 2) and corresponds to the 'Upper Siliceous Zone' of IGRS-IFP (1966). Since the attribution of the 'Upper Siliceous Zone' to the Albian–Cenomanian by IGRS-IFP (1966), very few detailed biostratigraphic studies have been carried out (e.g. Skourtsis-Coroneou, Solakius & Constantinidis, 1995). The Vigla Shale Member comprises limestone and chert beds interbedded with dark, greenish-grey shale, and is generally seen in the upper part of the Vigla Limestone Formation.

We examined rock outcrops of the Vigla Limestone Formation in the Gotzikas valley, south of Tsamantas village in NW Epirus, close to the border with Albania

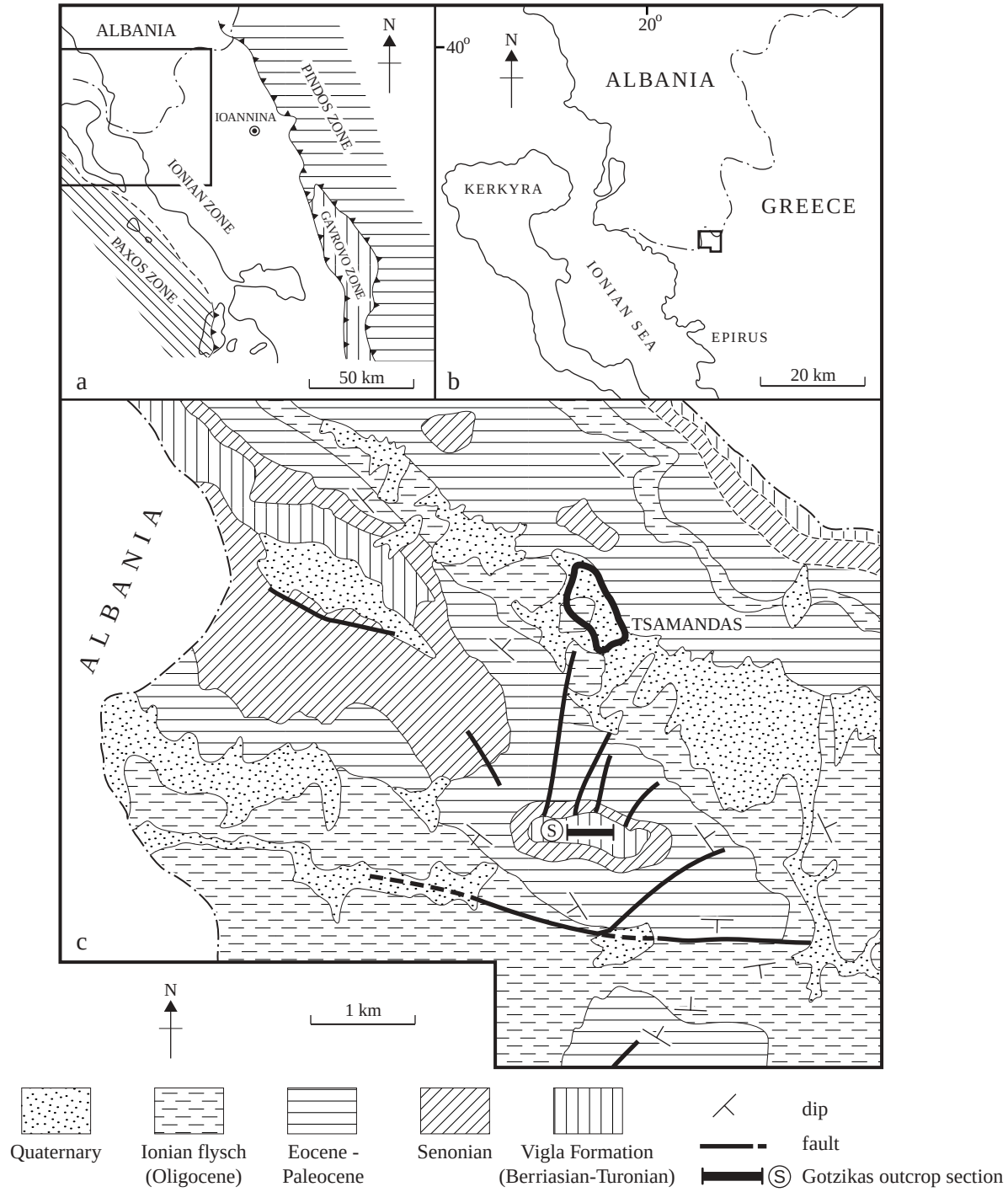

Figure 1. (a) The zones of NW Hellenides; (b) location of the study area; (c) simplified geological map of the study area (modified after IGRS-IFP, 1966).

(Fig. 1b, c). Here, the Vigla Shale Member is developed in the core of an anticline with its axis verging approximately along an E–W direction. Stratigraphically downwards, the sequence comprises Oligocene flysch, Eocene to Senonian limestones and the upper part of the Vigla Limestone Formation. Approximately 100 m of the Vigla Limestone Formation are seen, whereas the expected formation thickness in this area is 600 m (IGRS-IFP, 1966).

The upper *c*. 50 m of the Vigla Limestone in the Gotzikas section typically consists of a rhythmically alternating, thinly bedded limestone/black chert succession. Towards the lower 15–20 m of this interval, the limestone becomes more massive, pinkish-grey in colour and increasingly silicified. Within this lower portion we encountered a first, isolated black-shale horizon of a thickness of *c*. 15 cm. Silicified Vigla Limestone continues stratigraphically lower for another

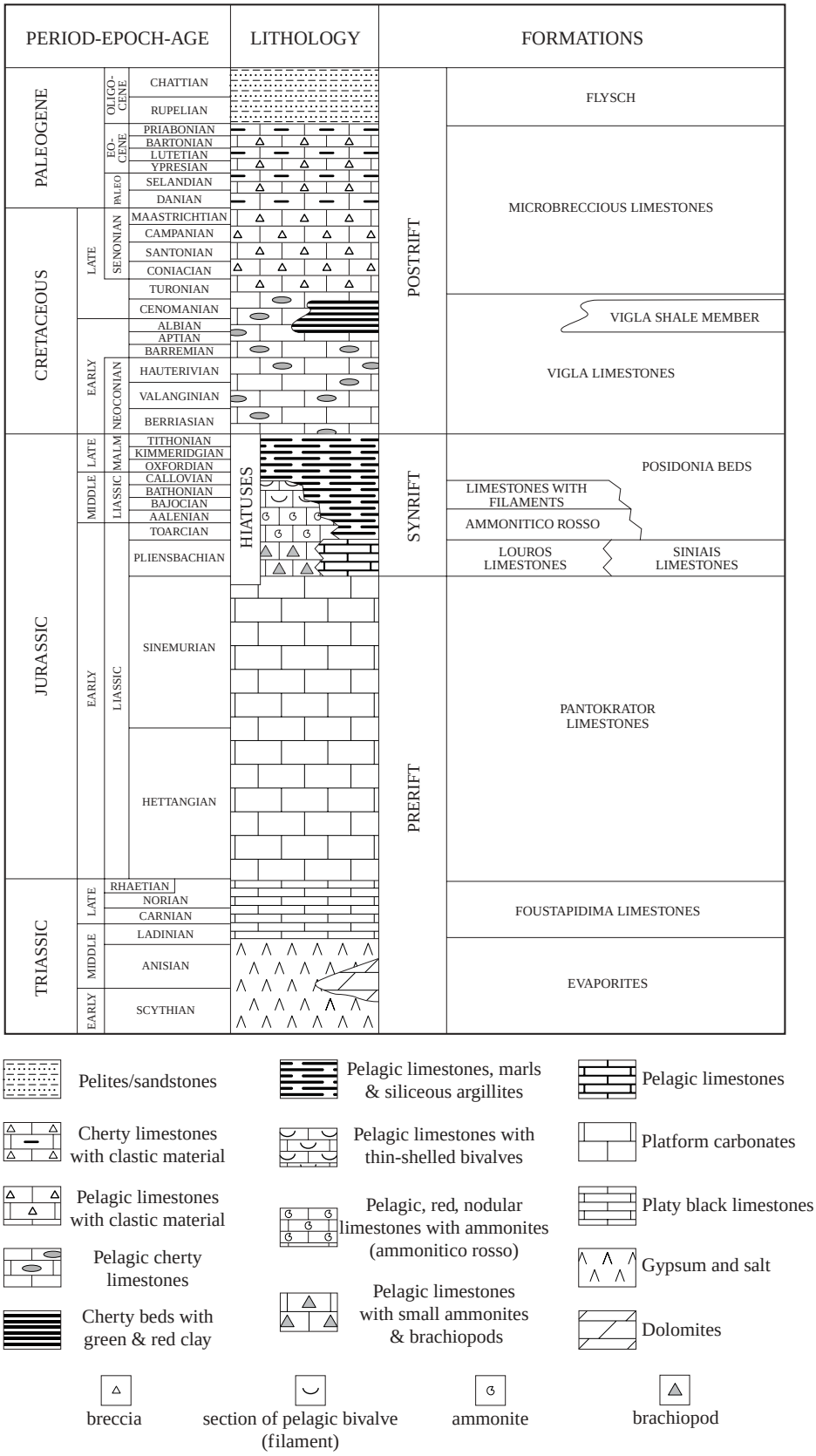

Figure 2. Representative stratigraphic column of the Ionian Zone (after Karakitsios, 1995).

8–10 m below this black shale. The series then appears to pass downwards to the Vigla Shale Member proper, although lack of exposure over the upper part of this shale-bearing section has hindered acquisition of a continuous lithological record.

In the lowermost *c*. 15 m of the examined outcrop, 20 individual organic-rich, marly horizons were seen, ranging in thickness from 10 to 40 cm. These layers are generally dark grey to black in colour, well laminated and free of evidence for bioturbation. They are interbedded with reddish-grey, 20–50 cm thick (marly) limestone beds, silicified in places and containing common intercalations of dark chert layers (5–10 cm thick).

4. Methods

4.a. Sampling

We collected hand-specimens approximately every 2 m through the upper *c*. 50 m of the Vigla Limestone Formation, including one sample from the stratigraphically uppermost black shale. Sampling on a decimetric to sub-decimetric scale was carried out for the lowermost *c*. 15 m of section (Vigla Shale Member proper), with a total of 25 samples being collected from the 20 organic-rich intervals themselves. All samples were powdered after careful screening to avoid contamination from weathering surfaces, local intense silicification or secondary carbonate veining.

4.b. Bulk organic geochemistry and C, O isotope determinations

Powdered samples were analysed for TOC and total carbonate contents, as well as bulk organic carbon and/or carbonate isotope ratios at the Departments of Earth Sciences and Archaeology, University of Oxford (Table 1). Duplicate TOC analyses were obtained for all organic carbon-rich samples, using a Strohlein Coulomat 702 device (for more details on this technique, see Jenkyns, 1988). Rock-Eval pyrolysis data (S0, S1, S2 and Tmax values) for the same samples were quantified using a LECO THA 200 Thermolytic Analyser at the University of Newcastle (Table 2). The standard deviations of duplicate analyses for S2 and Tmax, expressed as percentages of the average value, are $\pm 5\%$ and $\pm 4\%$ respectively.

For determinations of bulk organic carbon-isotope compositions, all TOC-rich samples were acidified with dilute HCl at ambient temperature to remove carbonate. Approximately 5–10 mg of the dried carbonate-free residues were weighed in tinfoil cups and placed in a Europa Scientific Limited CN biological sample converter connected to a 20–20 stable-isotope gas-ratio mass spectrometer. Carbon-isotope ratios were measured against a laboratory nylon standard, with a δ^{13}C value of -26.1 ± 0.2‰. Analytical results are presented in the usual δ notation, in ‰ deviation from the VPDB (Vienna Pee Dee Belemnite) standard.

Carbonate (C, O) isotope ratios for all collected samples were determined on CO_2 gas yielded after reaction with orthophosphoric acid at 90 °C, using a VG Isocarb device and Prism mass spectrometer. Normal corrections were applied and the results are reported using the δ notation v. VPDB. Calibration to VPDB was performed via our laboratory standard calibrated against NBS19 and Cambridge Carrara marble. Reproducibility of replicate analyses of standards was generally better than 0.1‰ for both carbon- and oxygen-isotope ratios.

4.c. Palynofacies analysis

Kerogen assemblages of ten selected organic-rich samples (including the sample representing the uppermost black shale) were isolated using non-oxidative palynological maceration with hydrochloric and hydrofluoric acids. The organic residues were then filtered via a 10 μm nylon mesh. Palynofacies analysis was undertaken at the University of Newcastle and involved the microscopic identification of opaque phytoclasts (black, oxidized woody debris), semi-opaque phytoclasts (brown, partially oxidized woody particles), translucent phytoclasts (fresh, non-oxidized woody debris), sporomorphs (land plant spores and pollen), marine algae (mainly dinoflagellate cysts) and amorphous organic matter (AOM) in transmitted white light (Table 3). Their percentages (based on particle number) were evaluated by counting at least 300 particles in each slide. The kerogen assemblages were also analysed in incident blue-light microscopy, using a blue light 450–490 nm excitation filter. The fluorescence intensity of AOM particles, which was used to evaluate the preservational state of kerogen, and consequently to infer the redox status of the depositional environment, was assessed using a six-point fluorescence scale (after Tuweni & Tyson, 1994; Tyson, 1995).

4.d. Compound-specific isotope methods

Rock powders of the ten organic-rich samples selected for palynofacies analyses were also solvent-extracted with a mixture of dichloromethane/methanol (9:1, v/v), using an automated solvent extractor (ASE). The total lipid extracts were subsequently separated by column chromatography into apolar and total polar fractions, and the apolar fractions were further separated into saturated and unsaturated fractions. Compositional information for all saturated apolar fractions was obtained using standard gas chromatography (GC) and gas chromatography–mass spectrometry (GC–MS) techniques. δ^{13}C measurements on selected compounds were performed after silicalite-adduction, to remove

Table 1. Bulk-rock geochemical and isotopic data of the Vigla Formation, NW Greece

Sample	TOC wt%	$CaCO_3$ wt%	$\delta^{13}C_{TOC}$ ‰	$\delta^{13}C_{carb}$ ‰	$\delta^{18}O_{carb}$ ‰	Depth* m	Lithology
C1				2.69	−1.89	55	Limestone-chert interbeds
C2				2.70	−2.04	54	”
C4				2.99	−1.87	53	”
C6				2.53	−2.09	52	”
C8				2.40	−2.11	51	”
C10				2.42	−2.05	50	”
C12				2.37	−2.07	49	”
C14				2.31	−2.05	47.5	”
C15				2.55	−1.94	46.5	”
C16				2.29	−2.10	45.5	”
C17				2.25	−2.14	44.5	”
C18				2.38	−1.99	43.5	”
C19				2.39	−2.01	42.5	”
C20				2.48	−1.72	41.5	”
C21				2.64	−1.63	40.5	”
C22				3.07	−1.81	39.5	”
C23				3.04	−1.89	38.5	”
C24				2.30	−1.94	36.5	”
C25				2.14	−1.81	34.5	”
C26				2.81	−1.87	32.5	”
C27				2.74	−1.74	30.5	”
C28				2.76	−1.67	28.5	”
C29				2.63	−1.77	26.5	”
C30				2.78	−1.55	24.5	”
C31				2.81	−1.49	22.5	”
C32				2.61	−1.44	20.5	Cherty limestone
C33				2.81	−1.27	18.5	”
C34				2.62	−0.78	16.5	”
C35†	28.87	23.25	−22.14	2.92	−1.32	14.8	Black shale
C36				2.97	−1.42	14.7	Cherty limestone
C37				3.79	−0.70	14.65	”
C39				3.39	−0.72	7.65	”
C40				2.07	−0.75	5.65	Marly limestone
C41	2.33	76.67	−26.61	2.23	−1.21	1.15	Organic C-rich shale
Observation gap* (taken also as ‘zero’ base line)							
V1				1.94	−0.96	−0.1	Marly limestone
V2				1.88	−0.98	−0.2	”
V3				2.10	−1.12	−0.3	”
V4a				2.16	−1.12	−0.36	”
V4b				2.23	−0.99	−0.42	”
V4c				2.05	−1.28	−0.48	”
V4d				2.19	−1.11	−0.54	”
V4e				1.81	−1.75	−0.6	”
V7				1.95	−1.34	−0.9	”
V8				1.80	−1.75	−1.02	”
V9				1.97	−1.24	−1.2	Light pink limestone
V11				2.18	−1.46	−1.4	”
V12a	1.58	76.58	−24.86	2.67	−1.43	−1.43	Organic C-rich shale
V12b				2.35	−1.83	−1.52	Light pink limestone
V12c	2.08	77.92	−25.84	2.58	−1.77	−1.55	Organic C-rich shale
V13	2.50	81.17	−25.75	2.61	−1.60	−1.6	”
V14				2.34	−1.52	−1.65	Light pink limestone
V16				1.57	−2.31	−1.9	”
V18				1.92	−1.59	−2	”
V19				2.05	−1.01	−2.1	”
V20				1.88	−1.18	−2.3	”
V21				2.06	−1.11	−2.5	”
V22				2.20	−1.19	−2.6	Marly limestone
V23a	1.41	91.33	−26.43	2.19	−1.16	−2.67	Organic C-rich shale
V23b	2.34	83.96	−26.25	2.24	−1.50	−2.75	”
V24				1.94	−1.42	−2.9	Light pink limestone
V25a				2.41	−1.33	−3	”
V25b				2.18	−1.19	−3.05	”
V26	3.35	61.67	−26.83	2.48	−1.53	−3.1	Organic C-rich shale
V27				2.34	−1.27	−3.3	”
V28				2.18	−1.49	−3.55	Light pink limestone
V29a	2.77	74.62	−26.10	2.64	−1.54	−3.65	Organic C-rich shale
V29b	2.15	84.67	−26.20	2.57	−1.67	−3.8	”
V29c	2.64	81.50	−25.97	2.70	−1.45	−3.9	”
V30				2.57	−1.46	−4	Light pink limestone

Table 1. Continued.

Sample	TOC wt%	$CaCO_3$ wt%	$\delta^{13}C_{TOC}$ ‰	$\delta^{13}C_{carb}$ ‰	$\delta^{18}O_{carb}$ ‰	Depth* m	Lithology
V32				2.08	−0.96	−4.1	”
V33				2.03	−0.78	−4.62	”
V34a				2.15	−1.00	−4.74	”
V34b				2.09	−1.03	−4.79	”
V35a				2.07	−1.44	−4.99	”
V35b				1.97	−1.31	−5.14	”
V38	1.88	79.58	−26.91	2.20	−1.97	−5.34	”
V39	1.08	74.42	−26.79	2.17	−1.45	−5.41	”
V41a	2.15	75.75	−27.88	2.05	−1.61	−5.61	Organic C-rich shale
V41b	3.19	72.92	−27.59	2.15	−1.52	−5.69	”
V42				2.00	−1.24	−5.79	Light pink limestone
V43a				2.03	−1.20	−6.04	Marly limestone
V43b				1.98	−0.94	−6.19	”
V45	2.57	54.08	−26.67	2.35	−1.50	−6.44	Organic C-rich shale
V46				2.05	−1.07	−6.79	Marly limestone
V47	4.42	67.83	−26.84	2.28	−1.55	−7.29	Organic C-rich shale
V48	1.54	83.42	−27.22	2.10	−1.01	−7.79	”
V49	2.39	80.08	−26.86	2.34	−1.44	−8.24	”
V50	3.61	53.35	−26.75	2.29	−1.34	−8.64	”
V51				2.32	−0.76	−8.7	Cherty/marly limestone
V52				2.32	−0.89	−9.5	”
V54	2.43	81.30	−25.96	2.62	−1.31	−10.05	Organic C-rich shale
V55				2.39	−1.03	−10.65	Cherty/marly limestone
V56	1.77	20.00	−26.37	2.35	−2.66	−10.72	Organic C-rich shale
V57				2.39	−0.68	−11.22	Cherty/marly limestone
V58	0.27	41.00	−26.52	2.46	−2.00	−11.52	Marly limestone
V59				2.53	−1.44	−12.32	Cherty/marly limestone
V60	2.29	84.50	−26.20	2.74	−1.37	−12.47	Organic C-rich shale
V61				2.58	−0.96	−12.97	Cherty/marly limestone
V62	6.33	59.92	−26.20	2.77	−1.30	−12.99	Organic C-rich shale
V63				2.48	−0.96	−13.17	Cherty/marly limestone
V64	2.77	81.12	−25.63	2.49	−1.14	−13.22	Organic C-rich shale

TOC: total organic carbon; carb: total carbonate (as calcite); †: uppermost black shale.
* Observation gap estimated to represent no more than 4–5 m stratigraphic thickness.

Table 2. Summary of bulk organic geochemical data for all 25 TOC-rich samples collected from the Vigla section in the Gotzikas locality

	TOC (wt%)	cf-TOC* (wt%)	HI (mg/g)	S2	T_{max} (°C)
Mean (n = 24, excl. UBS)	2.6	10.9	321	8.7	417
Range (excl. UBS)	1.1–6.3	2.2–16.3	171–450	2.4–29.1	402–425
UBS	28.9	37.6	529	152.7	420

* carbonate-free total organic carbon content; UBS – uppermost black shale.

Table 3. Summary of palynofacies data for ten TOC-rich samples selected from the Gotzikas section, including the uppermost black shale (UBS)

	Opaque phytoclasts (%)	Semi-opaque phytoclasts (%)	Translucent phytoclasts (%)	Sporomorphs (%)	AOM (%)	Marine algae (%)	Fluorescence scale
Mean (excl. UBS)	41.2	4.1	6.6	0.4	29.7	17.9	3.8
Range (excl. UBS)	31.5–51.3	1.4–5.7	1.9–14.1	0.0–0.7	18.0–37.2	13.8–26.1	3–5
UBS	33.2	2.8	4.4	0.0	56.3	3.2	5

Percentages expressed relative to the total population of particulate organic matter; AOM = Amorphous Organic Matter.

the abundant *n*-alkanes which may otherwise interfere with some of these compounds. Analyses were performed using a Thermofinnigan Delta C isotope-ratio monitoring gas chromatographer–mass spectrometer (irm-GC–MS) at the Royal Netherlands Institute for Sea Research (NIOZ). All compound-specific carbon-isotope measurements were carried out at least in duplicate, and the mean $\delta^{13}C$ values for each sample are presented in the usual δ notation with respect to the VPDB standard (Table 4).

Table 4. Compound-specific $\delta^{13}C$ data (in per mil v. VPDB) for the same ten organic carbon-rich Vigla samples as in Table 3

Sample	Norpristane	Pristane	Phytane	C29-sterane	C30-hopane	Monocyclic isoprenoid	C31-hopane
C35	−17.9	−20.5	−18.1	−27.8	−24.7	−15.0	−25.4
C41	nd	−32.1	−32.0	−30.3	−27.7		−29.8
V13	−30.9	−32.2	−32.8	−29.9	−26.3		−29.1
V23b	−32.2	−33.2	−33.0	−30.0	−27.1		−29.0
V29b	−30.6	−32.2	−32.5	−29.4	−26.1		−29.2
V38	−32.1	−32.7	−33.0	−29.6	−27.1		−29.8
V41b	−32.9	−32.9	−33.4	−29.7	−28.1		−29.7
V47	−31.4	−32.4	−32.2	−30.2	−27.3		−29.3
V54	−30.3	−31.4	−31.5	−28.6	−28.7		−28.9
V60	−31.5	−31.8	−31.3	−28.3	−28.1		−28.4

Data from all nine samples below the uppermost black shale (UBS. sample C35) represent duplicate means; values for the uppermost black shale sample are means of triplicate analyses: nd – not determined.

4.e. Biostratigraphic analyses

Calcareous nannofossil biostratigraphy was generated from 36 samples across the Gotzikas section, using standard smear slides (Bown & Young, 1998) and thin-sections. Planktonic foraminiferal biostratigraphy was based on the study of 63 thin-sections. All analyses were conducted at the Department of Earth Sciences 'Ardito Desio', University of Milan.

5. Results

5.a. Biostratigraphy

The distribution of biostratigraphically useful calcareous nannofossils and planktonic foraminifera across the Gotzikas section, and resulting age determinations, are summarized in Figure 3. Generally, a combination of poor preservation, low abundance and low diversity results in the absence of diagnostic taxa and thus hinders formulation of a complete biostratigraphic record through the entire section (Fig. 3). However, the interval −12 to −0.1 m (26.8 to 14.9 m below the uppermost black shale) may be assigned to the lower Aptian, based on the presence of the nannofossils *Assipetra infracretacea larsonii*, *Hayesites irregularis* and *Rucinolithus terebrodentarius youngii* (Larson *et al*. 1993; Tremolada & Erba, 2002), and the absence of nannofossils and planktonic foraminifera diagnostic of the upper Aptian.

In addition, the interval 22.5 to 32.5 m (7.7 to 17.7 m above the uppermost black shale) may be assigned to the middle Albian, based on the first occurrence of the nannofossil *Quadrum eneabrachium* and the presence of the planktonic foraminifer *Biticinella breggiensis* (Varol, 1992; Premoli Silva & Sliter, 1995). The overlying interval 36.5 to 38.5 m (21.7 to 23.7 m above the uppermost black shale) is uppermost Albian, based on the presence of the planktonic foraminifera *Rotalipora appenninica* and *Planomalina buxtorfi*, the presence of the nannofossil *Eiffellithus turriseiffelii* and the last occurrence of the nannofossil *H. irregularis* (Roth, 1978; Larson *et al*. 1993; Premoli Silva & Sliter, 1995). The first occurrence of the planktonic foraminifer *Rotalipora cushmani* at 44.5 m (29.7 m above the uppermost black shale) indicates the middle Cenomanian (Premoli Silva & Sliter, 1995).

5.b. Chemostratigraphy

Carbon- and oxygen-isotope profiles through the studied section are presented in Figure 4. Carbonate-carbon $\delta^{13}C$ values ($\delta^{13}C_{carb}$) show little stratigraphic variation, generally ranging between 2 and 2.5‰ over the lower 15 m (Vigla Shale Member), and between 2.5 and 3.0‰ in the upper 40 to 50 m (Vigla Limestone proper). Similarly, $\delta^{18}O$ values show a narrow range of *c*. −1 to −2‰ across essentially the entire section, although data exhibit significant scatter on a smaller scale.

With respect to the organic-rich samples, total carbonate is the main component in all samples below the uppermost black shale, with values generally around 75–80 wt% (as $CaCO_3$). TOC data for the same samples vary over the relatively narrow range of 1.1 to 6.3 wt%. However, the uppermost black shale shows a substantially reduced amount of bulk carbonate (23.3 wt%, as $CaCO_3$) and particularly high TOC content (28.9 wt%). In terms of bulk organic carbon $\delta^{13}C$ data ($\delta^{13}C_{org}$), the same black shale is also relatively enriched in ^{13}C with a $\delta^{13}C_{org}$ value of −22.1‰. This contrasts with the $\delta^{13}C_{org}$ values observed in all remaining samples lower in the section, which range between −28 and −25‰. It should be noted that $\delta^{13}C_{carb}$ values from both the uppermost black shale itself and from adjacent carbonate samples are also high, relative to average values from the remaining section (Fig. 4). It is debatable, however, whether these represent a primary isotopic signal or are the result of later diagenetic overprinting.

It is also noteworthy that there is no evidence for a negative carbonate isotope spike below the uppermost black shale in the Gotzikas section, as has been documented from immediately below both the lower

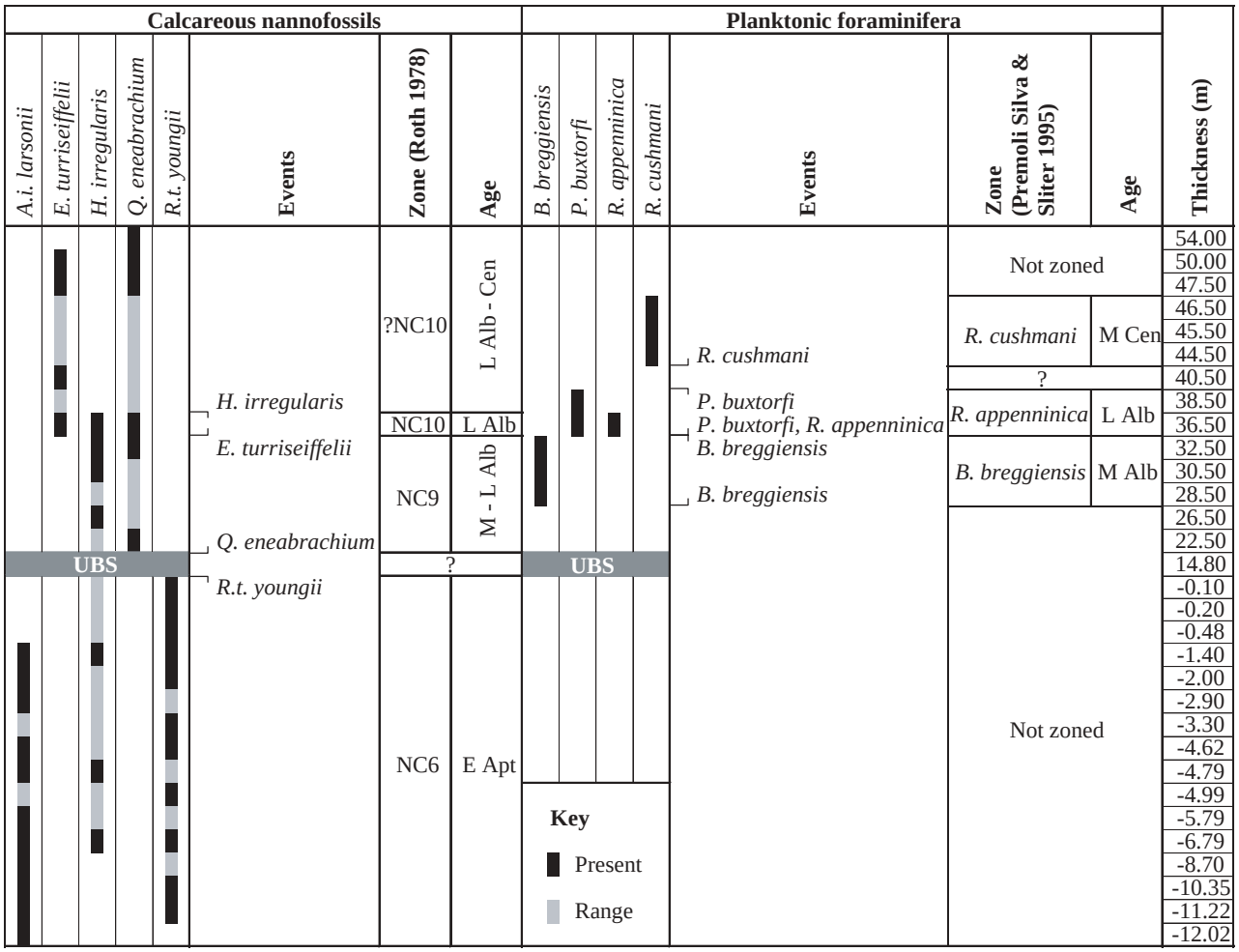

Figure 3. Summary of biostratigraphic information for the Gotzikas section, based on observed distributions of calcareous nannofossils and planktonic foraminifera. Whilst 36 samples were investigated for nannofossils and 63 for planktonic foraminifera, only those samples yielding age-diagnostic taxa are represented here. (UBS – uppermost black shale).

Albian Paquier Level (or OAE1b; for more details, see Section 6) in the Vocontian Basin of SE France and from a core in the Atlantic (Herrle, 2002). It is possible, however, that the critical level may have been lost to erosion, may not be exposed, or may have been missed due to the low sampling resolution over the interval in question.

5.c. Bulk organic geochemistry and palynofacies

Bulk organic geochemical and palynofacies data are summarized in Tables 2 and 3, respectively. All samples are very similar in terms of their organic facies characteristics, with the exception of the uppermost black shale. The mean Hydrogen Index (HI = mg S2/g TOC) is 321 (or 468 when computed from the linear regression of S2 v. TOC) and the HI values (ranging from 171 to 450) are broadly proportional to both the TOC and carbonate-free TOC contents. The uppermost black shale which, as mentioned earlier, is typified by a much higher TOC content (28.9 wt %), also has a higher HI value of 529. Using the plot of S2 v. TOC (after Langford & Blanc-Valleron, 1990), all samples are characterized as Type II kerogen (Fig. 5). The average Tmax value of 417 °C indicates that the samples are thermally immature, that is, stratigraphically above the oil window.

Ternary plots are routinely used in palynofacies analysis to investigate proximal-distal trends and redox conditions. The composition of the kerogen assemblages for the ten selected samples is summarized in the ternary diagram of AOM (Amorphous Organic Matter) v. phytoclasts v. palynomorphs (sporomorphs and marine algae) of Figure 6 (after Tyson, 1989, 1995). Palynofacies are dominated by small opaque phytoclasts, AOM and dinoflagellate cysts. This suggests a marine depositional environment quite distant from sources of fresh continental organic matter. The fluorescence of AOM is moderate to good (points 3 to 5 on the Fluorescence Scale), suggestive of dysoxic to anoxic conditions. The uppermost black shale sample exhibits the highest fluorescence and percentage of AOM (point 5 and 56 %, respectively), indicating better preservational conditions.

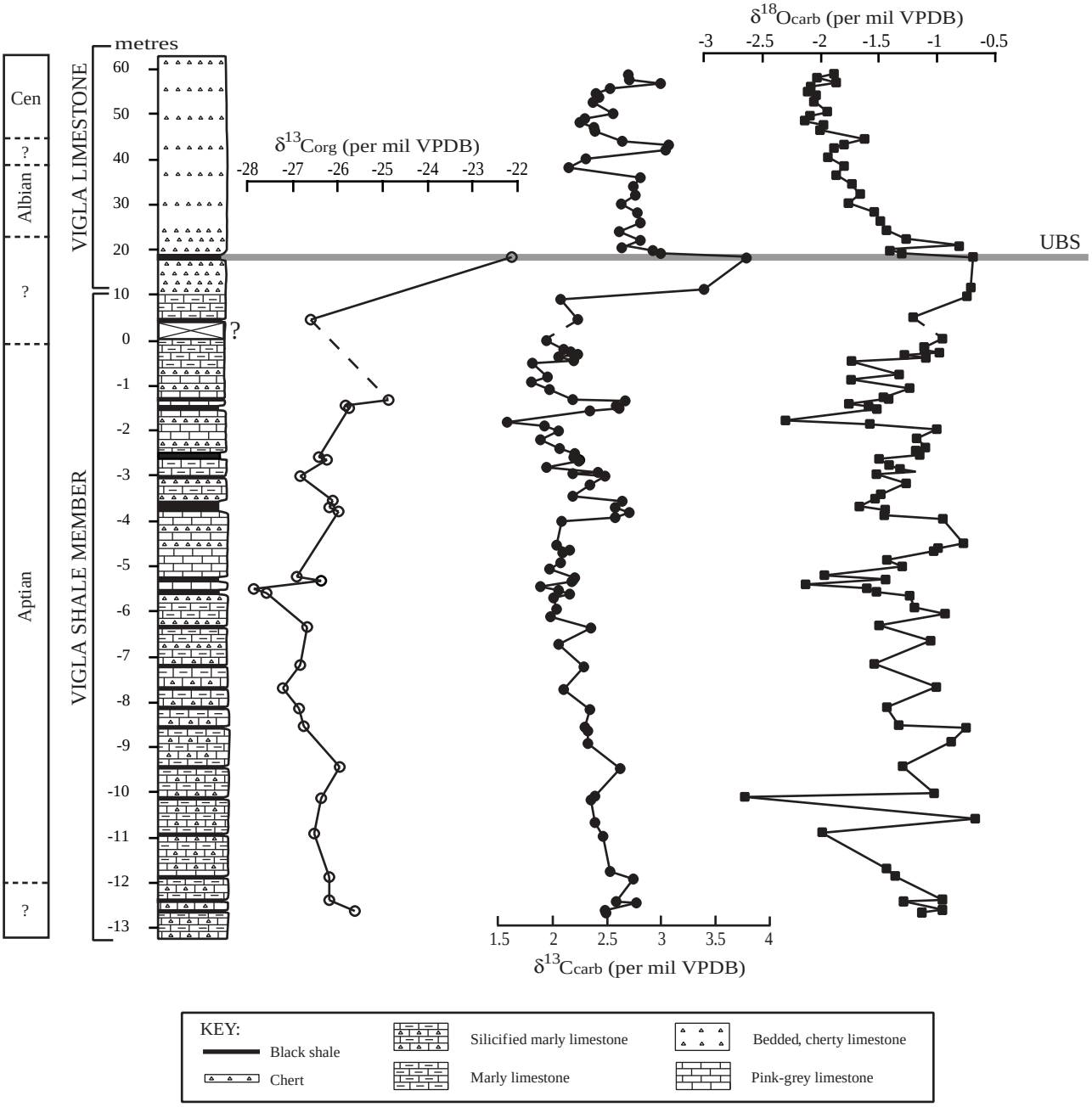

Figure 4. Lithostratigraphic log and bulk stable (C, O) isotope profiles through the Vigla section in the Gotzikas area. The uppermost black shale (UBS) is highlighted. Note the different scales used for the portions of the section above and below the observation gap (field observations indicate that this gap represents no more than 4–5 m of poorly exposed section).

5.d. Compound-specific isotope results

GC-MS data from the saturated apolar fractions of the same ten samples selected for palynofacies analyses show essentially identical composition, except for the sample representing the uppermost black shale. The components include mixtures of acyclic isoprenoids, *n*-alkanes, steroids and hopanoids (Fig. 7a, b) and to a much lesser extent alkylated thiophenes and naphthalenes. In contrast, the uppermost black shale contains relatively higher amounts of acyclic isoprenoids (especially norpristane) and, in addition to the aforementioned compounds, substantially elevated relative concentrations of monocyclic isoprenoids (Fig. 7a), the precise molecular structures of which are still unknown. Also, despite very low concentrations and strong co-elution effects, two other unusual isoprenoidal compounds, namely TME (2,6,15,19-tetramethylicosane) and PME (2,6,10,15,19-pentamethylicosane), were also detected in the uppermost black shale (Fig. 7a), on the basis of their corresponding mass spectra and characteristic retention times (Vink *et al*. 1998). All such isoprenoids have also been reported from the lower Albian, Niveau Paquier black shales from the

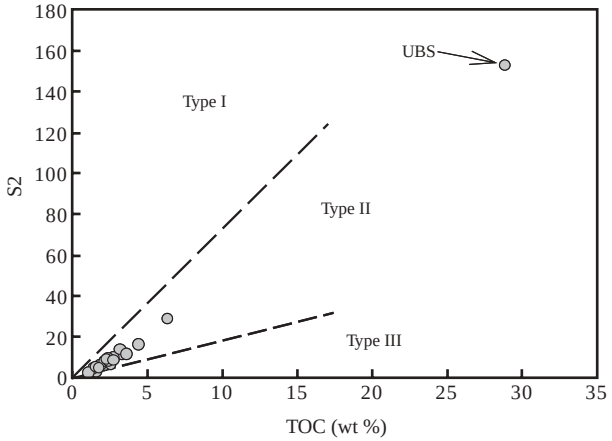

Figure 5. Binary plot of TOC v. S2 for all 25 TOC-rich samples from the Gotzikas section (kerogen type subdivisions after Langford & Blanc-Valleron, 1990). UBS – uppermost black shale.

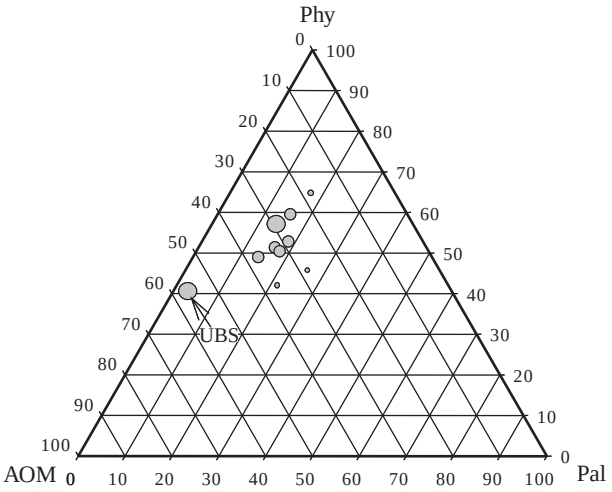

Figure 6. Ternary 'APP' plot (after Tyson, 1989, 1995) for ten selected TOC-rich samples, including the uppermost black shale (UBS). AOM – amorphous organic matter; Phy – total phytoclasts; Pal – palynomorphs (sporomorphs and marine algae). The size of the symbols is proportional to the fluorescence scale values (ranging from 3 to 5).

Vocontian Basin, SE France, as well as coeval organic carbon-rich sediments from ODP Site 1049C in the North Atlantic (Vink *et al*. 1998; Kuypers *et al*. 2002*a*), and are regarded as originating from marine archaea.

Compound-specific isotope data for selected organic compounds present in the saturated apolar fractions of the ten extracted samples are presented in Table 4. The nine samples stratigraphically below the uppermost black shale show essentially constant $\delta^{13}C$ compositions for pristane (−33 to −31‰), phytane (−34 to −30‰), norpristane (−34 to −30‰), steroids (e.g. C_{29}-sterane: −31 to −28‰) and hopanoids (e.g. C_{30}-hopane: −29 to −26‰; C_{31}-hopane (S+R): −30 to −28‰). The uppermost black shale sample, however, displays isoprenoid $\delta^{13}C$ values (pristane: −20.5‰; phytane: −18.5‰; norpristane: −17.9‰) that are substantially higher than those seen in the underlying TOC-rich samples. Furthermore, $\delta^{13}C$ values for monocyclic isoprenoids are also very high (up to −15‰ for monocyclic isoprenoid I; see also Fig. 7). These results contrast with the carbon isotope compositions of largely algal- and bacterial-derived biomarkers such as steranes and hopanes (Table 4), which exhibit only relatively small stratigraphic change, on the order of 2 to 4‰.

6. Discussion

It is known that at least two major Oceanic Anoxic Events (OAEs), that is, the early Aptian Selli event or OAE1a (e.g. Menegatti *et al*. 1998) and the Cenomanian–Turonian Bonarelli event or OAE2 (e.g. Arthur, Dean & Pratt, 1988; Tsikos *et al*. in press), represent episodes of global perturbation in both the marine inorganic and the marine/terrestrial organic carbon reservoirs, due to excess burial of organic matter. Such perturbations are commonly manifested in the form of positive isotopic excursions in both inorganic and organic carbon, by up to 2.5 and 6‰ respectively. At least a further three anoxic events of mostly (supra)regional geographical distribution have also been identified in the middle to upper Cretaceous (e.g. Leckie, Bralower & Cashman, 2002). Among these is the early Albian Paquier Event (or as variously termed, OAE 1b), a relatively short-lived (30–45 kyr) event of increased organic-carbon burial, that has been documented from the broader Tethys-Atlantic region (e.g. Bréhéret, 1985, 1997; Erbacher *et al*. 2001; Kuypers *et al*. 2001, 2002*a*; Herrle, 2002; Herrle *et al*. 2003*a*,*b*).

Planktonic foraminiferal and calcareous nannofossil stratigraphy across the Gotzikas section, in combination with the *c*. 4.5‰ isotopic shift seen in the bulk $\delta^{13}C_{org}$ record upwards in the section, provide a first indication that the uppermost part of the Vigla Shale Member examined herein (the uppermost black shale) may represent the lithological expression of the early Albian Paquier event. Direct evidence in this regard is provided by the compound-specific geochemical data (see Table 4, Fig. 8). Recent studies of the molecular organic geochemistry of lower Albian black shales from the Vocontian Basin, SE France (Niveau Paquier) and ODP Site 1049C, North Atlantic (Kuypers *et al*. 2001, 2002*a*), have shown that the Paquier Event is characterized by significant contributions of marine organic matter predominantly derived from chemoautotrophic archaea. This characteristic is firmly supported by the high $\delta^{13}C$ values (−18 to −16‰) observed in archaeal-derived isoprenoidal biomarkers, relative to biomarkers of more typical algal derivation (typically in the range −28 to −32‰), and thus distinguishes the Paquier Event from other Cretaceous OAEs.

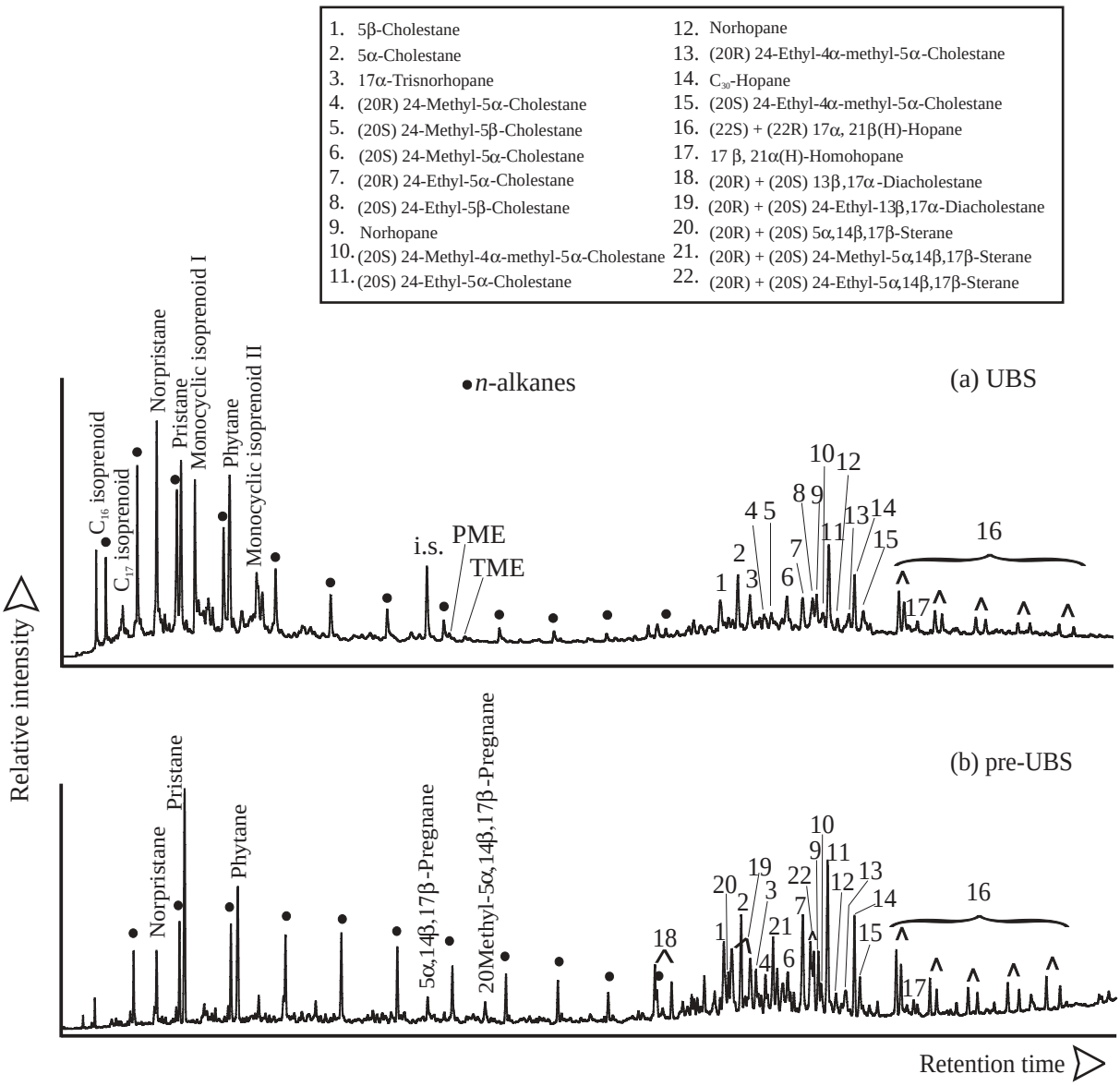

Figure 7. Total ion currents of the saturated apolar fractions for (a) the uppermost black shale (UBS) and (b) for one sample stratigraphically lower (V29b), indicating major compounds/compound groups present. Note the relative predominance of acyclic and monocyclic isoprenoids in the uppermost black shale (i.s. – internal standard).

The carbon-isotope profiles of Figure 8 illustrate striking similarities between the uppermost black shale and the Paquier black shale from ODP site 1049C (Kuypers *et al*. 2002*a*). The *c*. 4.5‰ isotopic shift in bulk $\delta^{13}C_{org}$ values between the uppermost black shale and underlying organic-rich units in the Gotzikas section can therefore be largely attributed to a change in the source of the organic matter, from predominantly marine algal to one where marine archaea became much more dominant. Respective isotopic shifts of at least 10‰ in acyclic isoprenoids appear to reflect such a mixed source (algal and archaeal), whereas values of up to −15‰ for monocyclic isoprenoids would indicate an almost exclusively archaeal derivation (Fig. 8). On the other hand, compounds of specifically algal origin (e.g. steranes) show little stratigraphic change in their $\delta^{13}C$ values (up to 4 per mil; see Fig. 8), as well as in their relative abundance. It is therefore unlikely that the isotopic shift seen in the upper part of the bulk $\delta^{13}C_{org}$ profile was caused exclusively by changes in isotopic fractionation of the primary algal biomass alone, and/or changes in the isotopic composition of dissolved inorganic carbon.

Estimations of the relative contribution of primary archaeal and algal sources to the uppermost black shale can only be tentative. Mass-balance calculations using the entire *c*. 4.5 shift in bulk $\delta^{13}C_{org}$ and end-member values of *c*. −26‰ for algae (based on the −30‰ of algal steranes corrected for the isotopic depletion of lipids in algae: Schouten *et al*. 1998) and −15‰ for archaea (based on the archaeal monocyclic isoprenoids) would lead to an estimate of an archaeal contribution

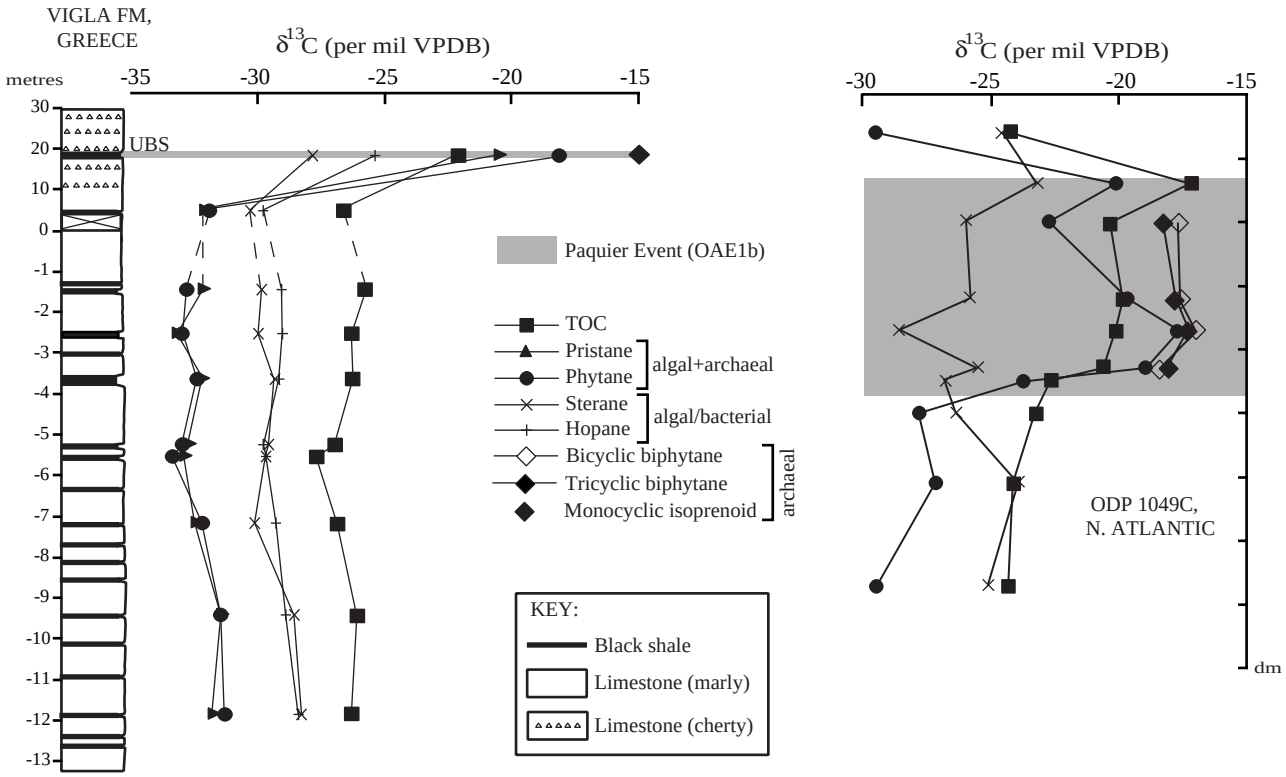

Figure 8. Carbon-isotope profiles for TOC, pristane, phytane, steranes, hopanes and archaeal isoprenoids, through the Vigla Shale Member of the Gotzikas section (this study) and ODP site 1049C from the North Atlantic (Kuypers *et al*. 2002*a*). TOC-rich intervals corresponding to the Paquier event (OAE1b) are highlighted. (UBS – uppermost black shale).

of *c*. 40%. This figure compares particularly well with that reported by Kuypers *et al*. (2002*a*) for the black shale of the Niveau Paquier in SE France. However, corresponding isotopic shifts of *c*. 1.5‰ in bulk carbonate and 2–4‰ in algal/bacterial biomarkers (steranes and hopanes) over the same stratigraphic interval, imply that approximately one third of the overall isotopic shift in the bulk organic carbon isotopic record may, in fact, be related to a respective change in the isotopic composition of the dissolved inorganic carbon reservoir. Therefore, the foregoing estimation of a primary archaeal contribution of *c*. 40% would only be a maximum one and should be reduced accordingly.

The recognition of a black shale attributable to the Paquier Event in the uppermost part of the Vigla Shale Member of the Ionian Basin also provides further insight into the chronostratigraphic extent of this interval. Traditionally, the upper portion of the Vigla Shale Member has been thought to span the late Cenomanian/early Turonian, though little biostratigraphic evidence has been presented to date in support of this (IGRS-IFP, 1966). Recent biostratigraphic and chemostratigraphic studies (Danelian *et al*. 2004) have demonstrated that the lower part of the Vigla Shale Member records the Selli Event/OAE1a (early Aptian). The present study complements this work, by setting a minimum age for the upper part of the Vigla Shale Member as Aptian to middle Albian.

7. Conclusions

The present study constitutes the first documentation of sediments deposited during the Paquier Event (OAE 1b) from the Ionian Basin of western Greece and complements similar recent work in older strata from the same area (Danelian *et al*. 2004). It also provides a new, revised minimum age constraint for the uppermost portion of the Vigla Shale Member which, until proven otherwise, appears to be considerably older than previously assumed (that is, early Aptian to middle Albian rather than Cenomanian/Turonian).

Our results also reinforce the notion that the Paquier Event constitutes a distinct episode in the Cretaceous geological record, whereby carbon-isotope anomalies of several per mil can be accounted for by variation in the source(s) of organic matter (that is, archaeal v. algal) in the marine realm. The Paquier equivalent in the Vigla section is in fact the third occurrence world-wide displaying these particular organic geochemical characteristics at the molecular level. Given that these horizons are geochemically so unusual they can be considered as time-equivalent, recording a specific biological event in the marine realm. By reference to the Niveuau Paquier in France and its equivalent in the Atlantic, the uppermost black shale in the Vigla section exposed near Gotzikas can hence be referred to the *Leymeriella tardefurcata* ammonite zone, the

Hedbergella planispira planktonic foraminiferal zone and the NC8B nannofossil zone of the early Albian (Bréhéret, 1997; Herrle, 2002).

Acknowledgements. This work was supported by the European Community's Improving Human Potential Program through the project 'C/T-Net – Rapid global change during the Cenomanian/Turonian oceanic anoxic event: examination of a natural climatic experiment in Earth history', under contract HPRN-CT-1999-00055, C/T-Net. The assistance and contributions of J. Cartlidge, T. O'Connell and S. Wyatt (TOC and bulk stable isotope analyses, Oxford), D. Sansom (drafting, Oxford), and M. Baas and W. I. C. Rijpstra (molecular analyses, NIOZ) are gratefully acknowledged. M. M. M. Kuypers (Max Planck Institute for Marine Microbiology, Bremen, Germany) is also thanked for providing selected data from ODP site 1049C from the North Atlantic, for the isotopic comparisons shown in Figure 8. Reviews by A. Y. Huc and H. Weissert greatly improved an earlier version of this manuscript.

References

ARTHUR, M. A., DEAN, W. E. & PRATT, L. M. 1988. Geochemical and climatic effects of increased marine organic carbon burial at the Cenomanian/Turonian boundary. *Nature* **335**, 714–17.

AUBOUIN, J. 1959. Contribution à l' étude géologique de la Grèce septentrionale: les confins de l' Epire et de la Thessalie. *Annales Géologiques des Pays Helléniques* **1**, 1–483.

BAUDIN, F. & LACHKAR, G. 1990. Géochimie organique et palynologie du Lias supérieur en zone ionienne (Grèce). Exemple d'une sédimentation anoxique conservée dans une paléo-marge en distension. *Bulletin de la Société Géologique de France* **8**, 123–32.

BERNOULLI, D. & JENKYNS, H. C. 1974. Alpine, Mediterranean and Central Atlantic Mesozoic Facies in relation to the early evolution of the Tethys. In *Modern and Ancient Geosynclinal Sedimentation* (eds R. H. Dott and R. H. Shaver), pp. 129–60. Society of Economic Paleontologists and Mineralogists, Special Publication no. 19.

BERNOULLI, D. & RENZ, O. 1970. Jurassic Carbonate Facies and New Ammonite Faunas from Western Greece. *Eclogae Geologicae Helvetiae* **63**, 573–607.

BOWN, P. R. & YOUNG, J. R. 1998. Techniques. In *Calcareous Nannofossil Biostratigraphy* (ed. P. R. Bown), pp. 16–28. London: Chapman and Hall.

BRÉHÉRET, J.-G. 1985. Indices d'un événement anoxique étendu à la Téthys alpine, à l'Albien inférieur (événement Paquier). *Comptes Rendus de l'Académie des Sciences, Paris, Séries II* **300**, 355–8.

BRÉHÉRET, J.-G. 1997. L'Aptien et l'Albien de la Fosse Vocontienne (bordures et basin): Évolution de la sédimentation et enseignements sur les événements anoxiques. *Publication Société Géologique du Nord* **25**, 614 pp.

CHIOTIS, S. 1983. Contribution of Organic Geochemistry to the Oil Exploration in Greece. *Proceedings 1st Geological Congress, Geological Society of Greece* **1**, 203–17.

DANELIAN, T., TSIKOS, H., GARDIN, S., BAUDIN, F., BELLIER, J. P. & EMMANUEL, L. 2004. Global and regional palaeoceanographic changes as recorded in the mid-Cretaceous (Aptian–Albian) sequence of the Ionian Zone (northwestern Greece). *Journal of the Geological Society, London* **161**, 703–10.

DOMMERGUES, J.-L., KARAKITSIOS, V., MEISTER, C. & BONNEAU, M. 2002. New ammonite data about the earliest syn-rift deposits (Lower Jurassic) in the Ionian Zone of N-W Greece (Epirus). *Neues Jahrbuch für Geologie und Paläontologie, Abhandlungen* **223**, 299–316.

DRAGASTAN, O., PAPANIKOS, D. & PAPANIKOS, P. 1985. Foraminifères, Algues et microproblematica du Trias de Messopotamos, Epire (Grèce continentale). *Revue de Micropaléontologie* **27**, 244–8.

ERBACHER, J., HUBER, B. T., NORRIS, R. D. & MARKEY, M. 2001. Increased thermohaline stratification as a possible cause for a Cretaceous oceanic anoxic event. *Nature* **409**, 325–7.

HERRLE, J. O. 2002. Paleoceanographic and paleoclimatic implications on Mid-Cretaceous black shale formation in the Vocontian Basin and the Atlantic: evidence from calcareous nannofossils and stable isotopes. *Tübinger Mikropaläontologische Mitteilungen* **27**, 114 pp.

HERRLE, J. O., PROSS, J., FRIEDRICH, O. & HEMLEBEN, C. 2003*a*. Short-term environmental changes in the Cretaceous Tethyan Ocean: micropalaeontological evidence from the early Albian Oceanic Anoxic Event 1b. *Terra Nova* **15**, 14–19.

HERRLE, J. O., PROSS, J., FRIEDRICH, O., KÖSSLER, P. & HEMLEBEN, C. 2003*b*. Forcing mechanisms for mid-Cretaceous black shale formation: evidence from the upper Aptian and lower Albian of the Vocontian Basin (SE France). *Palaeogeography, Palaeoclimatology, Palaeoecology* **190**, 399–426.

IGRS-IFP. 1966. *Etude Geologique de L' Epire (Grece Nord-Occidentale)*. Paris: Technip Editions, 306 pp.

JENKYNS, H. C. 1980. Cretaceous anoxic events: from continents to oceans. *Journal of the Geological Society, London* **137**, 171–88.

JENKYNS, H. C. 1988. The Early Toarcian (Jurassic) Anoxic Event: Stratigraphic, Sedimentary, and Geochemical Evidence. *American Journal of Science* **288**, 101–51.

JENKYNS, H. C. 1999. Mesozoic anoxic events and palaeoclimate. *Zentralblatt für Geologie und Paläontologie* **1997**, 943–9.

JENKYNS, H. C. 2003. Evidence for rapid climate change in the Mesozoic–Palaeogene greenhouse world. *Philosophical Transactions of the Royal Society, Series A* **361**, 1885–916.

JENKYNS, H. C., JONES, C. E., GRÖCKE, D. R., HESSELBO, S. P. & PARKINSON, D. N. 2002. Chemostratigraphy of the Jurassic System: applications, limitations and implications for palaeoceanography. *Journal of the Geological Society, London* **159**, 351–78.

JONES, C. E. & JENKYNS, H. C. 2001. Seawater strontium isotopes, oceanic anoxic events, and seafloor hydrothermal activity in the Jurassic and Cretaceous. *American Journal of Science* **301**, 112–49.

KARAKITSIOS, V. 1990. Chronologie et géometrie de l'ouverture d'un bassin et de son inversion tectonique: le bassin ionien (Epire, Grèce). *Mémoires Sciences de la Terre, Université Pierre et Marie Curie, Paris* **91–4**, 310 pp.

KARAKITSIOS, V. 1992. Ouverture et Inversion Tectonique du Basin Ionien (Epire, Grèce). *Annales Géologiques de Pays Helléniques* **35**, 85–318.

KARAKITSIOS, V. 1995. The Influence of Preexisting Structure and Halokinesis on Organic Matter Preservation and Thrust System Evolution in The Ionian Basin, Northwestern Greece. *American Association of Petroleum Geologists Bulletin* **79**, 960–80.

KARAKITSIOS, V., DANELIAN, T. & DE WEVER, P. 1988. Datation par les radiolaires des Calcaires à Filaments, Schists à Posidonies supérieurs et Calcaires de Vigla (zone ionienne, Epire, Grèce) du Callovien au Tithonique terminal. *Comptes Rendus de l'Académie des Sciences, Paris, Séries II* **306**, 367–72.

KARAKITSIOS, V. & KOLETTI, L. 1992. Critical revision of the age of the basal Vigla Limestones (Ionian Zone, Western Greece) based on Nannoplankton and Calpionellids, with Paleogeographical consequences. In *Proceedings of the Fourth International Nannoplankton Association Conference (Prague, 1991)* (eds B. Hamersmid and J. Young), pp. 165–77. *Knihovnika Zemniho Plynu a Nafty* **14a**.

KARAKITSIOS, V. & RIGAKIS, N. 1996. New Oil Source Rocks Cut in Greek Ionian Basin. *Oil & Gas Journal*, Feb. 12, OGJ SPECIAL, 56–9.

KARAKITSIOS, V. & TSAILA-MONOPOLIS, S. 1988. Données nouvelles sur les niveaux supérieurs (Lias inférieur-moyen) des Calcaires de Pantokrator (zone ionienne moyenne, Epire, Grèce continentale). Description des Calcaires de Louros. *Revue de Micropaléontologie* **31**, 49–55.

KARAKITSIOS, V. & TSAILA-MONOPOLIS, S. 1990. Données nouvelles sur les niveaux inférieurs (Trias supérieur) de la serie calcaire ionienne en Epire (Grèce continentale). Conséquences stratigraphiques. *Revue de Paleobiologie* **9**, 139–47.

KUYPERS, M. M. M., BLOKKER, P., ERBACHER, J., KINKEL, H., PANCOST, R. D., SCHOUTEN, S. & SINNINGHE DAMSTÉ, J. S. 2001. Massive expansion of marine Archaea during a mid-Cretaceous Oceanic Anoxic Event. *Science* **293**, 92–4.

KUYPERS, M. M. M., BLOKKER, P., HOPMANS, E. C., KINKEL, H., PANCOST, R. D., SCHOUTEN, S. & SINNINGHE DAMSTÉ, J. S. 2002*a*. Archaeal remains dominate marine organic matter from the early Albian oceanic anoxic event 1b. *Palaeogeography, Palaeoclimatology, Palaeoecology* **185**, 211–34.

KUYPERS, M. M. M., PANCOST, R. D., NIJENHUIS, I. A. & SINNINGHE DAMSTÉ, J. S. 2002*b*. Enhanced productivity led to increased organic carbon burial in the euxinic North Atlantic basin during the Cenomanian/Turonian oceanic anoxic event. *Paleoceanography* **17**, 1–13.

LANGFORD, F. F. & BLANC-VALLERON, M. M. 1990. Interpreting Rock-Eval pyrolysis data using graphs of pyrolyzable hydrocarbons *vs* total organic carbon. *American Association of Petroleum Geologists Bulletin* **74**, 799–804.

LARSON, R. L. & ERBA, E. 1999. Onset of the mid-Cretaceous greenhouse in the Barremian–Aptian: Igneous events and the biological, sedimentary, and geochemical responses. *Paleoceanography* **14**, 663–78.

LARSON, R. L., FISCHER, A. G., ERBA, E. & PREMOLI SILVA, I. 1993. *APTICORE-ALBICORE: A Workshop Report on Global Events and Rhythms of the mid-Cretaceous, 4–9 October, 1992, Perugia, Italy*. 56 pp.

LAUBSCHER, H. P. & BERNOULLI, D. 1977. Mediterranean and Tethys. In *The ocean basins and margins, Vol. 4A, The eastern Mediterranean* (eds A. E. M. Nairn, W. H. Kanes and F. G. Stehli), pp. 1–28. New York: Plenum Press.

LECKIE, R. M., BRALOWER, T. J. & CASHMAN, R. 2002. Oceanic anoxic events and plankton evolution: Biotic response to tectonic forcing during the mid-Cretaceous. *Paleoceanography* **17**, 10.1029/2001PA000623, 29 pp.

MENEGATTI, A. P., WEISSERT, H., BROWN, R. S., TYSON, R. V., FARRIMOND, P., STRASSER, A. & CARON, M. 1998. High-resolution δ^{13}C stratigraphy through the early Aptian "Livello Selli" of the Alpine Tethys. *Paleoceanography* **13**, 530–45.

NEUMANN, P. & ZACHER, W. 2004. The Cretaceous sedimentary history of the Pindos Basin (Greece). *International Journal of Earth Sciences (Geologische Rundschau)* **93**, 119–31.

PANCOST, R. D., CRAWFORD, N., MAGNESS, S., TURNER, A., JENKYNS, H. C. & MAXWELL, J. R. 2004. Further evidence for the development of photic-zone euxinic conditions during Mesozoic Oceanic Anoxic Events. *Journal of the Geological Society, London* **161**, 353–64.

POMONI-PAPAIOANNOU, F. & TSAILA-MONOPOLIS, S. 1983. Petrographical, Sedimentological and Micropaleontological studies of an evaporite outcrop, West of Ziros lake (Epirus-Greece). *Rivista Italiana di Paleonologia e Stratigraphia* **88**, 387–400.

PREMOLI SILVA, I. & SLITER, W. V. 1995. Cretaceous planktonic foraminiferal biostratigraphy and evolutionary trends from the Bottaccione section, Gubbio, Italy. *Palaeontographica Italica* **82**, 1–89.

RENZ, C. 1955. *Die vorneogene Stratigraphie der normalsedimentären Formationen Griechenlands*. Institute of Geological Subsurface Research, Athens, 637 pp.

RIGAKIS, N. & KARAKITSIOS, V. 1998. The source rock horizons of the Ionian Basin (NW Greece). *Marine and Petroleum Geology* **15**, 593–617.

ROTH, P. H. 1978. Cretaceous nannoplankton biostratigraphy and oceanography of the northwestern Atlantic Ocean. In *Initial Reports of the Deep Sea Drilling Project* **44** (W. E. Benson, R. E. Sheridan *et al.*), pp. 731–60. Washington: US Government Printing Office.

SCHLANGER, S. O. & JENKYNS, H. C. 1976. Cretaceous oceanic anoxic events: causes and consequences. *Geologie en Mijnbouw* **55**, 179–84.

SCHOUTEN, S., KLEIN BRETELER, W., BLOKKER, P., SCHOGT, N., RIJPSTRA, W. I. C., GRICE, K., BAAS, M. & SINNINGHE DAMSTÉ, J. S. 1998. Biosynthetic effects on the stable carbon isotopic compositions of algal lipids: Implications for deciphering the carbon isotopic biomarker record. *Geochimica et Cosmochimica Acta* **62**, 1397–1406.

SINNINGHE DAMSTÉ, J. S. & KÖSTER, J. 1998. A euxinic southern North Atlantic Ocean during the Cenomanian/Turonian oceanic anoxic event. *Earth and Planetary Science Letters* **158**, 165–73.

SKOURTSIS-CORONEOU, V., SOLAKIUS, N. & CONSTANTINIDIS, I. 1995. Cretaceous stratigraphy of the Ionian Zone, Hellenides, western Greece. *Cretaceous Research* **16**, 539–58.

TREMOLADA, F. & ERBA, E. 2002. Morphometric analyses of Aptian *Assipetra infracretacea* and *Rucinolithus terebrodentarius* nannoliths: implications for taxonomy, biostratigraphy and paleoceanography. *Marine Micropaleontology* **44**, 77–92.

TSIKOS, H., JENKYNS, H. C., WALSWORTH-BELL, B., PETRIZZO, M. R., FORSTER, A., KOLONIC, S., ERBA, E.,

PREMOLI SILVA, I., BAAS, M., WAGNER, T. & SINNINGHE DAMSTÉ, J. S. 2004. Carbon-isotope stratigraphy recorded by the Cenomanian-Turonian Oceanic Anoxic Event: correlation and implications based on three key-localities. *Journal of the Geological Society, London* **161**, 711–20.

TUWENI, A. O. & TYSON, R. V. 1994. Organic facies variations in the Westbury Formation (Rhaetic, Bristol Channel, S. W. England). *Organic Geochemistry* **200**, 1001–14.

TYSON, R. V. 1989. Late Jurassic palynofacies trends, Piper and Kimmeridge Clay Formations, UK onshore and offshore. In *Northwest European Micropaleontology and Palynology* (eds D. J. Batter and M. C. Keen), pp. 135–72. British Micropalaeontological Society Series. Chichester: Ellis Horwood.

TYSON, R. V. 1995. *Sedimentary Organic Matter: Organic facies and palynofacies*. London: Chapman & Hall, 516 pp.

VAROL, O. 1992. Taxonomic revision of the Polycyclolithaceae and its contribution to Cretaceous biostratigraphy. *Newsletters on Stratigraphy* **27**, 93–127.

VINK, A., SCHOUTEN, S., SEPHTON, S. & SINNINGHE DAMSTÉ, J. S. 1998. A newly discovered norisoprenoid, 2,6,15,19-tetramethylicosane, in Cretaceous black shales. *Geochimica et Cosmochimica Acta* **62**, 965–70.